ME:4086 Mechanical Engineering Design
Inverted Pendulum Educational Display

Author:
Will Martin

Teammates:
Anvay Pradhan, Jacob Fuhrmeister, and Charles Vazquez

May 20, 2022

Contents

1 Abstract

The goal of this project was to design an inverted pendulum control system for an education displayed housed in the University of Iowa's Seamans Center. The display should showcase the knowledge learned by a mechanical engineering student and get new students excited about engineering. The inverted pendulum system should be interactive for observers but also take safety into consideration. This group began the project by designing a working inverted pendulum simulation and prototype hardware. The prototype hardware is physically able to stabilize the pendulum in the unstable equilibrium, however the control systems designed in simulation do not work due to real-world factors such as friction and feedback inaccuracies.

2 Introduction

* Section contributions from Anvay Pradhan, Jacob Fuhrmeister, and Charles Vazquez

2.1 Need Statement

The University of Iowa College of Engineering (CoE), housed in the Seamans Center, is home to several hundred engineering undergraduates, graduate students, faculty, and staff. Despite the concentration of engineering education in a single building, there exist very few educational displays demonstrating the type of work students complete as part of their studies. Further, as [1] explains, the demonstration of current students' ideas and experiences is instrumental in the recruitment of prospective students. Thus, this project's purpose is to design an educational display to showcase principles taught in engineering classes. In particular, the display is to be an inverted pendulum system that is able to self-stabilize in an unstable state given a perturbation. The final designs will display the capabilities of senior mechanical engineering students and act as a tool to motivate future potential students to attend the University of Iowa.

2.2 Project Scope and Goals

The project system includes a physical design, a dynamics model, and a controller. A typical inverted pendulum consists of a cart and pendulum system with two degrees of freedom as shown in Figure 1. The cart has one translational degree of freedom along axis x while the pendulum has one rotational degree of freedom given by angle θ. The state of the cart, $[x, \dot{x}]$ is controllable while the state of the pendulum $[\theta, \dot{\theta}]$ is uncontrollable but observable.

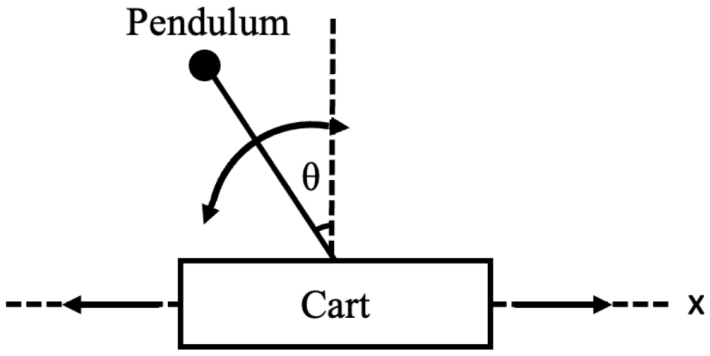

Figure 1: The inverted pendulum system. The two independent degrees of freedom are shown with arrows.

The final design based on the prototype made during this project will be installed inside the University of Iowa Seamans Center in a location that can be easily visited by current and prospective students. The installation should have a physical interactive component. This function will include user-controlled destabilization and stabilization, and perturbations.

3 Dynamics

3.1 Overview

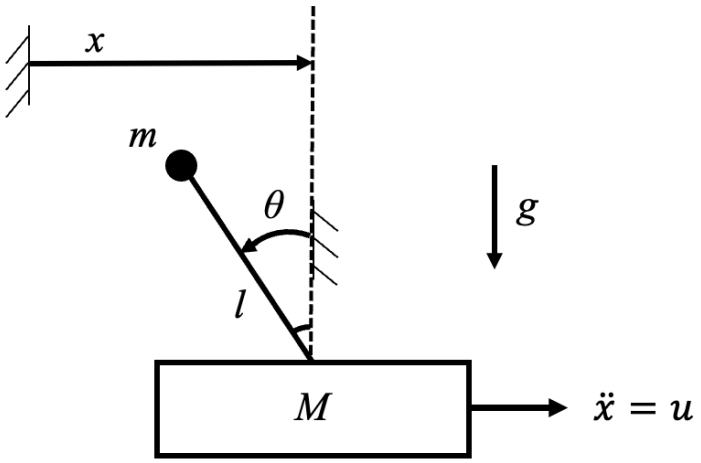

Figure 2: Inverted pendulum system diagram

An inverted pendulum consists of a cart and pendulum system with two degrees of freedom as shown in Figure 2. The cart has one translational degree of freedom along axis x while the pendulum has one rotational degree of freedom given by angle θ. The control input, u, is the acceleration of the cart along the x-axis. The system's physical parameters and their estimated values are shown in Table 1.

Table 1: Physical Parameters

Parameter	**Notation**	**Value**	**Units**
Mass of Pendulum	m	0.10	kg
Length of Pendulum	l	0.25	m
Mass of Cart	M	0.31	kg
Gravity	g	9.81	m/s^2
Pulley Radius	r	0.015	m

In this section, three sets of governing equations are solved for. Each set of equations will be used to design a specific controller in Section 5.

3.2 Nonlinear Governing Equation

The nonlinear governing equation for the inverted pendulum system was derived using the Lagrangian in Equation 1. The Lagrangian, L, is the difference between the systems kinetic energy, T, and potential energy, V.

$$L = T - V \tag{1}$$

To solve for the system's kinetic and potential energy, the position and velocity of the point mass on top of the pendulum were derived as shown in Equation 2.

$$
\begin{aligned}
x_p &= -l\sin\theta \\
\dot{x_p} &= -l\cos\theta\dot{\theta} + \dot{x} \\
y_p &= l\cos\theta \\
\dot{y_p} &= -l\sin\theta\dot{\theta}
\end{aligned}
\tag{2}
$$

The system's total kinetic energy is shown in Equation 3 and the total potential energy is shown in Equation 4.

$$
\begin{aligned}
T &= \frac{1}{2}M\dot{x}^2 + \frac{1}{2}m(\dot{x_p}^2 + \dot{y_p}^2) \\
&= \frac{1}{2}(M+m)\dot{x}^2 + \frac{1}{2}ml^2\dot{\theta}^2 - ml\cos\theta\dot{\theta}\dot{x}
\end{aligned}
\tag{3}
$$

$$
\begin{aligned}
V &= mgy_p \\
&= mgl\cos\theta
\end{aligned}
\tag{4}
$$

Equation 3 and Equation 4 were substituted into Equation 1 to derive the Lagrangian in Equation 5.

$$
L = \frac{1}{2}(M+m)\dot{x}^2 + \frac{1}{2}ml^2\dot{\theta}^2 - ml\cos\theta\dot{\theta}\dot{x} - mgl\cos\theta \tag{5}
$$

The Euler–Lagrange equation was used to solve for the equations of motion with respect to the angle θ in Equation 6 with F_{ex} representing the external damping force on the pendulum rotation point.

$$
\begin{aligned}
F_{ex} &= \frac{d}{dt}\frac{\partial L}{\partial\dot{\theta}} - \frac{\partial L}{\partial\theta} \\
&= ml^2\ddot{\theta} - ml\cos\theta\ddot{x} - mgl\sin\theta
\end{aligned}
\tag{6}
$$

With the moment of inertia defined by Equation 7, Equation 6 was rearranged to give the final equation of motion in Equation 8.

$$
I = ml^2 \tag{7}
$$

$$
\ddot{\theta} = \frac{ml\cos\theta\ddot{x} + mgl\sin\theta + F_{ex}}{I} \tag{8}
$$

The equation of motion with respect to the x-axis is simply given by Equation 9 if it is assumed that the given input acceleration, u, directly corresponds to the actual acceleration of the cart. To make this assumption the motor most be able to overcome any damping within the rail system. This topic is covered further in Section 6.2.

$$
\ddot{x} = u \tag{9}
$$

The state space variables for the system are defined in Equation 10. The full nonlinear dynamics are shown in Equation 11.

$$
\mathbf{x} = \begin{bmatrix} x_1 \\ x_2 \\ x_3 \\ x_4 \end{bmatrix} = \begin{bmatrix} x \\ \dot{x} \\ \theta \\ \dot{\theta} \end{bmatrix} \tag{10}
$$

$$\dot{\mathbf{x}} = \begin{bmatrix} \dot{x_1} \\ \dot{x_2} \\ \dot{x_3} \\ \dot{x_4} \end{bmatrix} = \begin{bmatrix} x_2 \\ u \\ x_4 \\ \frac{mlcos(x_3)u + mglsin(x_3) + F_{ex}}{I} \end{bmatrix} \tag{11}$$

In this study, the system is simplified by assuming no damping within the pendulum rotation joint as shown in Equation 12.

$$F_{ex} = 0 \tag{12}$$

3.3 Linear Governing Equation

The linear full system dynamics were derived. The linearized system can be represented in state-space form as generalized in Equation 13.

$$\dot{\mathbf{x}} = \mathbf{A}\mathbf{x} + \mathbf{B}u \tag{13}$$

The system was linearized about the unstable equilibrium in Equation 14 using a first order Taylor Series to produce the full system linear dynamics in Equation 15

$$\begin{bmatrix} x \\ \theta \end{bmatrix} = \begin{bmatrix} 0 \\ 0 \end{bmatrix} \tag{14}$$

$$\dot{\mathbf{x}} = \begin{bmatrix} \dot{x_1} \\ \dot{x_2} \\ \dot{x_3} \\ \dot{x_4} \end{bmatrix} = \begin{bmatrix} 0 & 1 & 0 & 0 \\ 0 & 0 & 0 & 0 \\ 0 & 0 & 0 & 1 \\ 0 & 0 & \frac{mgl}{I} & 0 \end{bmatrix} \begin{bmatrix} x_1 \\ x_2 \\ x_3 \\ x_4 \end{bmatrix} + \begin{bmatrix} 0 \\ 1 \\ 0 \\ \frac{ml}{I} \end{bmatrix} u \tag{15}$$

3.4 Isolated Cart Governing Equation

Finally, the dynamics for the isolated cart with no pendulum were derived in state-space form as shown in Equation 16.

$$\dot{\mathbf{x}} = \begin{bmatrix} \dot{x_1} \\ \dot{x_2} \end{bmatrix} = \begin{bmatrix} 0 & 1 \\ 0 & 0 \end{bmatrix} \begin{bmatrix} x_1 \\ x_2 \end{bmatrix} + \begin{bmatrix} 0 \\ 1 \end{bmatrix} u \tag{16}$$

4 Control

4.1 Overview

The inverted pendulum is controlled by two controllers with a switch condition. The nonlinear controller swings the pendulum upright within the linear region defined in Equation 17. The system then switches to the linear controller for stabilization. The control design is based around work shown in [4] and [2].

$$-\frac{\pi}{9} < \theta < \frac{\pi}{9} \tag{17}$$

4.2 Nonlinear Controller Design

The nonlinear controller was derived from the energy-based, positive definite Lyapunov Function in Equation 18. In Equation 18, the total energy of the pendulum is represented by E as defined in Equation 19 and the energy of the pendulum at the equilibrium point is E_0 which is defined to be 0 for this system as shown in 20

$$
\begin{aligned}
V &= \frac{1}{2}(E - E_0)^2 \\
&= \frac{1}{2}\Delta E^2
\end{aligned}
\tag{18}
$$

$$
E = \frac{1}{2}I\dot{\theta}^2 + mgl(cos(\theta) - 1) \tag{19}
$$

$$
E_0 = 0 \tag{20}
$$

The first time derivative of the Lyapunov Function was derived using the nonlinear dynamics from Equation 11 as follows in Equation 21.

$$
\begin{aligned}
\dot{V} &= \Delta E \dot{E} \\
&= \Delta E \dot{\theta}(I\ddot{\theta} - mgl\sin\theta) \\
&= \Delta E \dot{\theta}(I(\frac{ml\cos\theta u + mgl\sin\theta}{I}) - mgl\sin\theta) \\
&= \Delta E \dot{\theta} ml\cos\theta u
\end{aligned}
\tag{21}
$$

Equation 22 shows the controller design to make Equation 21 negative semi-definite as shown in Equation 23.

$$
u = -k_{nonlinear}\Delta E\dot{\theta}cos(\theta) \tag{22}
$$

$$
\dot{V} = -k_{nonlinear}ml(\Delta E\dot{\theta}cos(\theta))^2 \tag{23}
$$

The controller in Equation 22 is able to swing the pendulum into the linear region at a low angular velocity, but unable to stabilize at the unstable equilibrium position. This analysis was done in simulation using the nonlinear system dynamics and an ODE solver. This is shown in Figure 3.

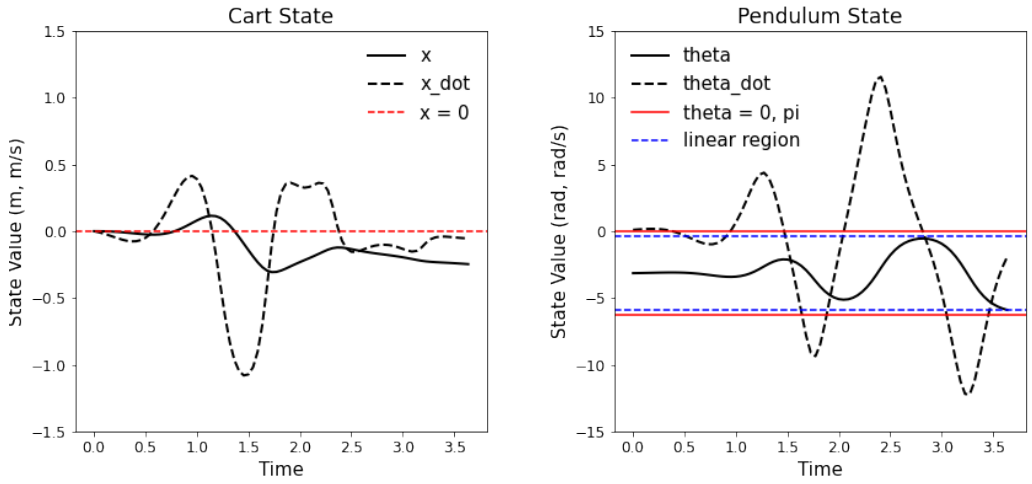

Figure 3: Nonlinear controller simulation results

This controller however does not stabilize the cart's position about the center of the rail at $x = 0$. To fix this issue, an additional term was added to the control value based on the dynamics of the cart in Equation 16. These dynamics were used with a pole placement strategy to find a $k_{linear\ cart}$ to stabilize the cart about

$x = 0$. The full nonlinear control signal is shown in Equation 24. Figure 4 shows a simulation of this control signal.

$$u = -k_{nonlinear}(E - E_0)\dot{\theta}cos(\theta) - k_{linear\ cart}\mathbf{x} \tag{24}$$

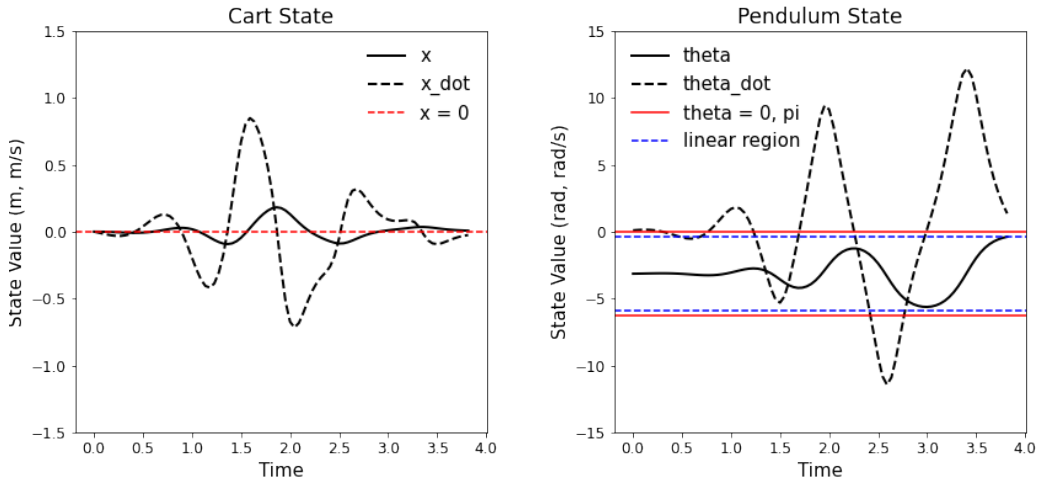

Figure 4: Nonlinear controller with x-axis stabilization simulation results

4.3 Linear Controller Design

Once the nonlinear controller swings the pendulum into the linear region, the linear controller takes over to stabilize the system. This controller was designed around the linearized dynamics in Equation 15. A simple proportional controller was used with a gain, k_{linear}, found using an LQR. The final controller is shown in Equation 25.

$$u = -k_{linear}\mathbf{x} \tag{25}$$

A simulation of the linear controller was made. In this simulation the initial state values were taken from the final state values of the nonlinear controller once it passed into the linear region. This simulation is shown in Figure 5.

4.4 Gain Values

Each of the gain values found for the values in Table 1 are shown in Table 2.

Table 2: Gain Values

Gain	**Value**
$k_{nonlinear}$	3.1
$k_{linear\ cart}$	$[2, 3]^T$
k_{linear}	$[-1, -2.1, 26.2, 4.3]^T$

4.5 State Estimation

The pendulum system's state y must be fully observable to control the system. This is defined by Equation 26 and 27.

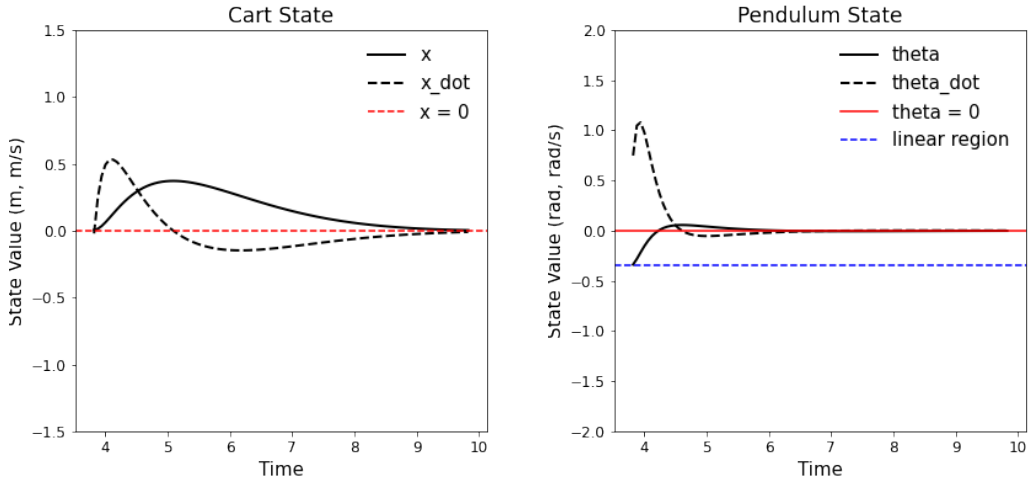

Figure 5: Linear controller simulation results

$$\mathbf{y} = \mathbf{C}\mathbf{x} + \mathbf{D}u \tag{26}$$

$$\mathbf{y} = \begin{bmatrix} 1 & 0 & 0 & 0 \\ 0 & 1 & 0 & 0 \\ 0 & 0 & 1 & 0 \\ 0 & 0 & 0 & 1 \end{bmatrix} \begin{bmatrix} x_1 \\ x_2 \\ x_3 \\ x_4 \end{bmatrix} \tag{27}$$

The state value x was found by counting the steps taken by the stepper motor and the value θ was found by counting the pulses received from the encoder. $\dot{x}$ and $\dot{\theta}$ were both found by numerically differentiating the state values x and θ and then averaging the values over the past 3 time steps. This leads to time lag in the reading for these values.

5 Mechanical Design

5.1 Overview

The mechanical system prototype was designed for easy manufacturing and assembly. A CAD model of the design is shown in Figure 6 and a photograph of the system is shown in Figure 7.

The frame was design from 80-20 extruded aluminum and mounted to a piece of plywood. A 80-20 compatible slider was used driven by a NEMA 23 stepper motor (See Section 6.2). 3D printed parts hold the stepper motor, mount the encoder and pendulum to the cart, mount the limit switches, and hold the belt idler-pulley. The belt can easily be tensioned by sliding the idler-pulley along the 80-20 aluminium. Additionally, the top rail features mechanical stops to prevent the cart from running into the limit switch bodies if the limit switches are not functioning properly.

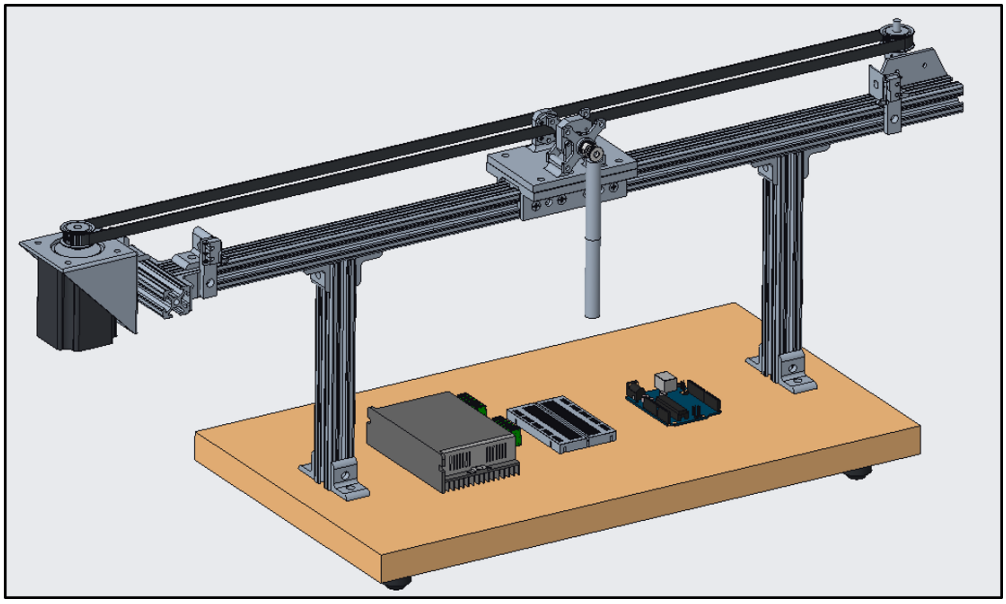

Figure 6: Mechanical design CAD model

Figure 7: Mechanical design photograph

5.2 Motor Selection

A stepper motor was selected over a typical brushed or brushless motor for accurate controllability. The type of stepper motor was chosen so that the maximum torque at the maximum required RPM could be handled without skipping steps. The maximum values endured by the system in simulation with the physical parameters given in Table 1 are shown in Table 3.

Table 3: Estimated Max Dynamics Values

Parameter	Notation	Value	Units
Acceleration	u_{max}	6.60	m/s^2
Position	x_{max}	0.38	m
Velocity	$\dot{x}_{max}$	0.85	m/s
Angle	θ_{max}	π	rad
Angular Velocity	$\dot{\theta}_{max}$	12.21	rad/s

The estimated maximum torque experienced by the motor is expressed in Equation 28. In this equation, $M_{friction\ equivalent}$ is added to the mass of the cart to make an estimated account for the frictional force of the rail on the cart.

$$\begin{aligned} \tau_{max} &= (M + M_{friction\ equivalent}) * u_{max} * r \quad with \quad M_{friction\ equivalent} \approx 0.50kg \\ \tau_{max} &= (0.31 + 0.50)\ kg * 6.6\ m/s^2 * 0.015\ m = 0.08\ Nm \end{aligned} \tag{28}$$

The estimated maximum RPM needed from the motor is determined in Equation 29.

$$RPM_{max} = \frac{\dot{x} = 0.85\ m}{s} * \frac{1\ rot}{2\pi * .015\ m} * \frac{60\ s}{1\ min} = 541.13\ RPM \tag{29}$$

This operating range was plotted on several stepper motor pull-out torque curves to verify that the motor would be able to handle the control signal needed. The plots for a NEMA 17 and the chosen NEMA 23 motors are shown in Figure 8. Both motors are able to operate at the required conditions; however, the NEMA 23 has a much larger factor of safety leading it to be chosen.

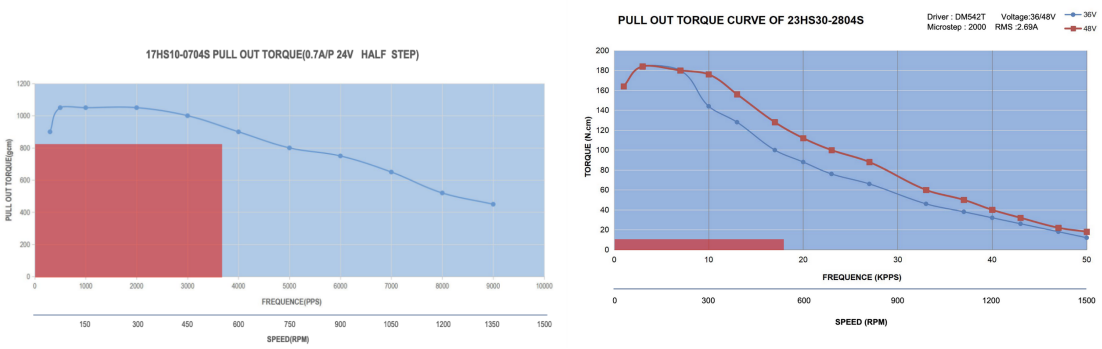

Figure 8: Pullout torque curves for NEMA 17 [Left] and NEMA 23 [Right]. Pendulum operating range is highlighted in red

5.3 Encoder Selection

A quadrature relative encoder was selected for the project. Specifically part number AMT103-2048-N4000-S from CUI devices. This encoder has 2048 pulses per revolution (PPR) and by counting the pulses using quadrature resolution the output can be counted at 8192 counts per revolution (CPR). This leads to an angle resolution of 0.044 deg. Additionally, this encoder was selected for easy mounting options and low internal friction.

5.4 Schematic

The schematic for the electronics system can be seen in Figure 9. The digital pin connections in this figure match those used in the provided code.

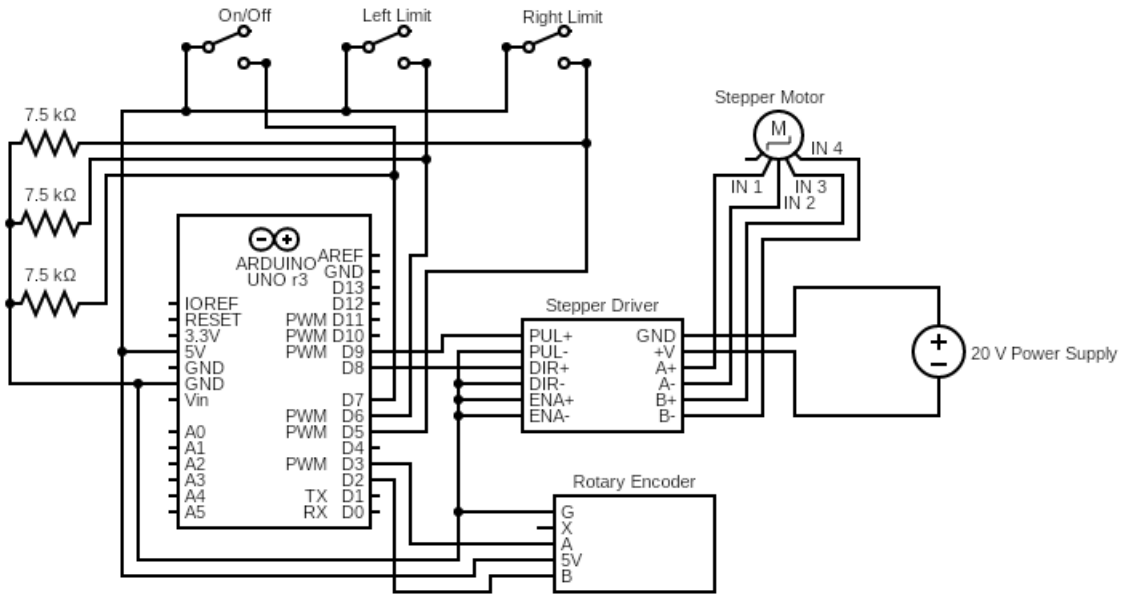

Figure 9: Pendulum system schematic

6 Alternative Designs

6.1 General Mechanical Design

When initially designing the mechanical system, two major design decisions were made. First, it was decided that a translational cart should be used rather than a rotational cart. This decision was made using the decision matrix shown in Figure 10.

The second decision made was to use a single link pendulum arm rather than a multi-link arm. This decision was also made using a decision matrix. This matrix is shown in Figure 11.

6.2 Control

Two different nonlinear control schemes were attempted before the current system was decided upon. Initially, a controller was designed based on the Lyapunov function shown in Equation 30. However, this controller was abandoned due to complexity and the team's inability to find a control signal that made the Lyapunov function negative definite or negative semi-definite.

$$L = \frac{1}{2}x^T x \tag{30}$$

The second control scheme that was attempted was based on [3]. This controller used a sign function to determine the control signal. Although this control signal worked. It's output had many discrete jumps which would make it very difficult to implement in a real-world system. Instead, this design was abandoned for the control scheme shared earlier which produces a smooth control output.

Requirement	*Weight*	*Concept 1:* Translational cart	*Concept 2:* Rotational cart
Demonstration of engineering principles	0.2	5	5
Visual appeal	0.3	5	3
Noise pollution	0.1	5	4
Cost	0.1	4	2
Interactive-ness	0.1	4	3
Ease of manufacturing	0.2	4	2
Total	**1.0**	**4.6**	**3.2**

Figure 10: Physical cart design decision matrix

Requirement	*Weight*	*Concept 1:* Single link pendulum	*Concept 2:* Multi-link pendulum
Demonstration of engineering principles	0.2	3	4
Visual appeal	0.3	4	4
Noise pollution	0.1	5	3
Cost	0.1	4	2
Interactive-ness	0.1	3	3
Ease of manufacturing	0.2	4	4
Total	**1.0**	**3.8**	**3.6**

Figure 11: Physical pendulum design decision matrix

6.3 Rail System

The initial rail system used a precisely machined rail and cart pair that was designed for incredibly low friction. Once this item was received the team realized that the cart only offered low friction if it was loaded. Since our design did not include a significant load on the cart, it was replaced with the 80-20 rail and cart system that was easily obtained, although high in friction.

6.4 Encoder

The encoder used in the final prototype was also not the original one ordered. Originally the team planned to use an absolute rotatory encoder. This encoder was shipped broken and had to be returned. The new encoder used in the final design has a input shaft hole instead of a shaft for better loading.

7 Standards

* Section contributions from Anvay Pradhan

Four standards were considered to guide the design of the inverted pendulum system and the Engineering Design Specification (EDS).

7.1 Code of Federal Regulations (CFR): PART 1239 - SAFETY STANDARD FOR GATES AND ENCLOSURES

This standard is equivalent to the ASTM F1004-21: Standard Consumer Safety Specification for Expansion Gates and Expandable Enclosures standard. The standard was referenced when writing the EDS section on the inverted pendulum display case. The standard details accessibility of interactive components of enclosures. This includes what a sharp edge is and how to avoid creating them, the maximum force allowed for interactive components, usable material types, and appropriate mounts.

7.2 Fire Code 2015 of Iowa

Section 314 of this Fire Code was studied. This section gives advice on indoor displays. The code specifically states that "free, immediate, and unobstructed access" should be given to exits surrounding the display.

7.3 Iowa Electrical Examining Board (IEEB) - ELECTRICAL CODE AND UPDATES

This standard adopts the 2020 National Electrical Code (NEC) as issued by the National Fire Protection Agency (NFPA). The Seamans Center where the display will eventually be installed qualifies as building under public entity and therefore is a public indoor space. This standard details voltage and current standards for operational displays in public indoor spaces.

7.4 The University of Iowa Design Standards & Procedures

The final standard is produced by the University of Iowa Facilities Management team. This guide details guidelines specific to the University of Iowa and any designs pertaining to its physical image. Specifically, this code provides structural, accessibility, and environmental standards as well as aesthetic choices that the university would like all things related to their image to follow. Section 8.3.1.8.3 was specifically studied as is pertains to display cases.

8 Future Work

There are many aspects of the project that needed continual work. First, the safety enclosure needs to be carefully designed to encase the final inverted pendulum display to keep observers safe. Next, the control scheme needs to be update to include the friction of the real-world system. This means that the friction in the physical model needs to be measured. The team believes that this term must be added to the control stack to be able to translate the simulation to the real-world. Additionally, the hardware code needs to be updated to run more accurately in real time. This could be done by using a multi-core microprocessor or chaining two Arduino UNOs together so that the timings of the stepper motor can be executed separately from the encoder readings and control signal calculations. Finally, the physical system could be improved to more accurately read the state of the pendulum and cart. An encoder could be added to the stepper motor belt so that a skipped step will not result in a misreading. Also, an Extended Kalman Filter (EKF) could be used to find $\dot{\theta}$ and $\dot{x}$ with more accuracy and without the time lag from numerical differentiation.

References

[1] Michael E. Burns. Recruiting prospective students withstories: How personal stories influence the process of choosing auniversity. *Communication Quarterly*, 63(1):99–118, 2015.

[2] H. Hanekam. Implementation and control of an inverted pendulum on a cart. In *The Arctic University of Norway*, 2021.

[3] Bakhtyar Abdullah Sharif and Ahmet Ucar. State feedback and lqr controllers for an inverted pendulum system. In *2013 The International Conference on Technological Advances in Electrical, Electronics and Computer Engineering (TAEECE)*, pages 298–303, 2013.

[4] N. Vestergaard. Swing-up and stabilization of a cart pendulum and twin pendulum system. In *Aalbord University*, 2018.